

Enhanced optical absorbance of hydrophobic Ti thin film: role of surface roughness

Jyoti Jaiswal¹, Amit Sanger¹, Ashwani Kumar¹, Satyendra Mourya¹, Samta Chauhan¹, Ritu Daipuriya², Manpreet Singh² and Ramesh Chandra^{1*}

¹Nano Science Laboratory, Institute Instrumentation Centre, Indian Institute of Technology Roorkee, Roorkee 247667, India

²Photonics Division, Terminal Ballistics Research Laboratory, Chandigarh 160030, India

*Corresponding author. E-mail: ramesfic@iitr.ac.in

Received: 07 July 2015, Revised: 29 December 2015 and Accepted: 05 March 2016

ABSTRACT

In the present work, structural, morphological, optical and wettability properties of DC magnetron sputtered titanium (Ti) thin films have been investigated. The nanostructured Ti thin films were deposited on glass and silicon substrates at various deposition angles, $\theta_D = 0^\circ, 30^\circ, 45^\circ$ and 60° . HCP structure of Ti thin films with preferred peak orientations (100) and (002) were revealed from XRD. It was observed that as the deposition angle increases, film thickness (~260 - 100 nm) as well as average crystallite size (~27 - 11 nm) of Ti thin films decrease. Significant changes in topography of the films, with change in deposition angle, have been observed. The optical and wettability results suggested that transmission, reflection, absorption and water contact angle of Ti thin films are strongly influenced by deposition angle due to change in its surface roughness. The large near infrared (NIR) absorbance (~66 - 75%) was found for the sample deposited at $\theta_D = 30^\circ$, which exhibited hydrophobic (~94.6°) nature with high surface roughness (~28 nm). Copyright © 2016 VBRI Press.

Keywords: Ti thin films; sputtering; surface roughness; NIR absorbance; hydrophobicity.

Introduction

For many decades, the physical and chemical properties of nanostructured metal, metal oxide, metal sulphide, metal nitride and metal doped semiconductor/dielectric thin films have been widely investigated in order to reveal their fundamental processes and to examine possible technological applications [1–6]. In particular, thin films of titanium (Ti) and its alloys have continued to capture the researcher's interest owing to their unique optical, wettable, mechanical, thermal, electrical, magnetic and chemical properties [7–12]. Thin films of Ti were found to possess excellent properties, such as, low density, good mechanical strength, high corrosion resistance, low electrical resistivity, good chemical and thermal stability, high melting point, biocompatibility and good optical absorption. These properties of Ti makes it a highly promising material for wide scientific applications like aerospace, biomedical industries, single electron devices, gas and infrared sensors, integrated optics, VLSI technology and micro-electro-mechanical system (MEMS) based devices [13–20].

Moreover, the optical properties of Ti thin films, such as, reflectance (R) and absorbance (A), also make this material interesting for applications like solar cells, transmission laser joining and photonic devices [9, 13, 21, 22]. James E. Kennedy, in 2001, proposed the use of Ti thin film as a photon absorbing layer on glass/quartz window for laser initiation of insensitive energetic materials [23]. The interaction of NIR (700-1100 nm) radiation with Ti thin films results into heating of the surface and production of

plasma thrust, thereby, initiating the insensitive energetic materials at low threshold energy [21, 24]. Therefore, optimization of deposition parameters for enhanced NIR absorption of Ti thin films are required. This can enable the development of safe, flexible, light-weight, high-performance, cost-effective and multifunctional laser detonators for insensitive energetic materials that are difficult to achieve with present light absorbers.

Recent studies have shown that the microstructure of Ti thin films such as surface morphology, grain size, porosity as well as film thickness strongly influences their properties like mechanical, optical, electrical and thermal [15, 25–29]. A lot of work has been reported so far in order to grow Ti thin films using different deposition techniques [9, 12, 29, 30]. Among these, we have chosen magnetron sputtering to fabricate Ti thin films due to its versatility and proven reproducibility. In magnetron sputtering technique, along with other parameters, the deposition angle can also act as a tuning parameter to control the microstructure and porosity of fabricated films. There are many reports in which PVD methods have been used to study the dependence of microstructural, roughness, and optical properties of metal and metal oxide thin films on the deposition angle [30–37]. In addition, for biomedical applications, the wettability plays an important role in the optimization of adhesion, spreading and proliferation of biological cells [16,38]. However, the role of deposition angle on wettability and optical properties of Ti thin film is still lacking in the literature [22,26,28–31,38–40].

The motivation of the present work is to study the wettability and enhance the absorbance of Ti thin film in

the NIR region. The absorbance and wettability are highly dependent on surface roughness and can be varied by the deposition angle [30,31,35]. Therefore, in the present work, we have studied wettability and optical properties of the Ti thin films as a function of deposition angle. We have achieved the improved NIR absorption ($\sim 66\text{-}75\%$) for the sample having maximum surface roughness (~ 28 nm) and water contact angle ($\sim 94.6^\circ$), deposited at $\theta_D = 30^\circ$.

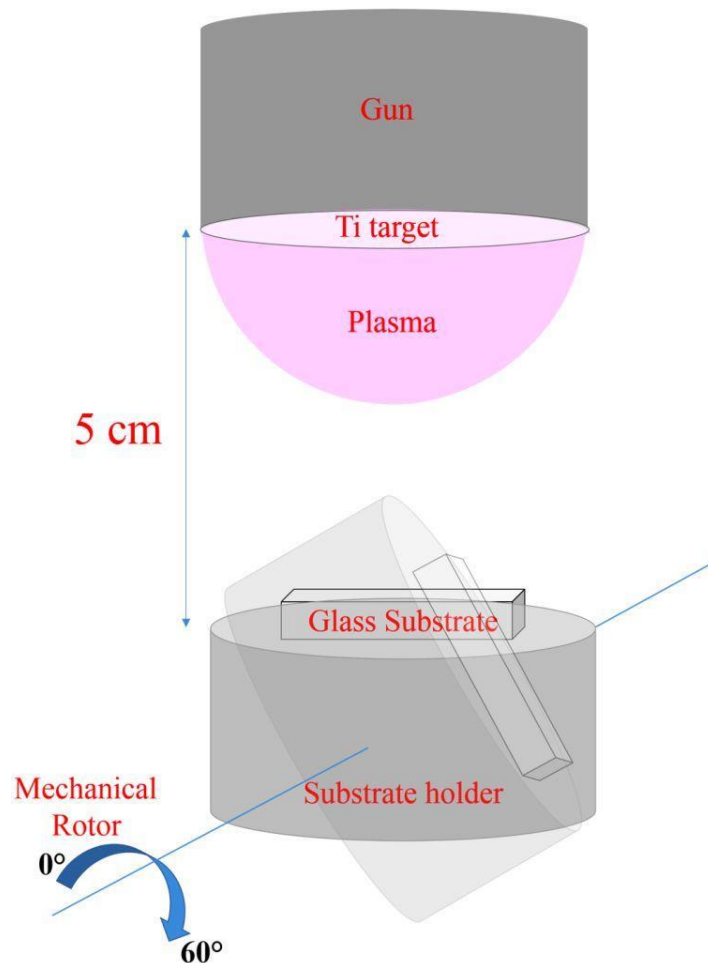


Fig. 1. Schematic diagram of deposition system for Ti thin films, deposited at various angles ($0^\circ \leq \theta_D \leq 60^\circ$).

Experimental

Synthesis

Ti thin films were deposited on glass and Si substrates at various deposition angles, $\theta_D = 0^\circ, 30^\circ, 45^\circ$ and 60° by employing DC magnetron sputtering in a custom designed 30.48 cm diameter sputtering chamber (Excel Instruments, Mumbai). Sputtering target (5 cm diameter and 0.5 cm thick) of Ti with purity of 99.95 % has been used for deposition. Sputtering was carried out at constant Ar (20 sccm) flow. The Ti film was prepared at room temperature. The DC power densities for Ti target were 4 W/cm^2 . All depositions were carried out at a fixed substrate to target distance of 5 cm and deposition time of 5 min. Before the deposition, the vacuum chamber was initially evacuated to 3×10^{-6} Torr using a turbo molecular pump backed by rotary pump. Thereafter, high purity inert

gas Ar (99.99 %) was introduced into chamber. The base pressure before deposition was 3×10^{-6} Torr and the argon pressure were kept at 5 mTorr during sputtering. Deposition angle was controlled by sample position controller (Dynamic control system) mounted with substrate holder as shown in **Fig. 1**. Before deposition, the Ti target was pre-sputtered for 5 min to remove the surface contamination of the target and controlled uniformity.

Characterizations

The Ti thin films were analyzed by employing Grazing angle X-ray diffractometer (GA-XRD, Bruker D8 Advanced) for crystal structure determination and average particle size calculations. Field emission scanning electron microscope (FE-SEM, FEI Quanta 200F) was used to get surface morphology and cross section of Ti thin films. Atomic force microscope (AFM, NT-MDT NTEGRA) was used to find surface morphology and surface roughness of Ti thin films. The water droplet contact angles were measured by sessile drop method using Kruss DSA 100 easy drop. The optical properties of Ti thin films were determined using Cary Varian 5000 UV-Vis-NIR spectrophotometer.

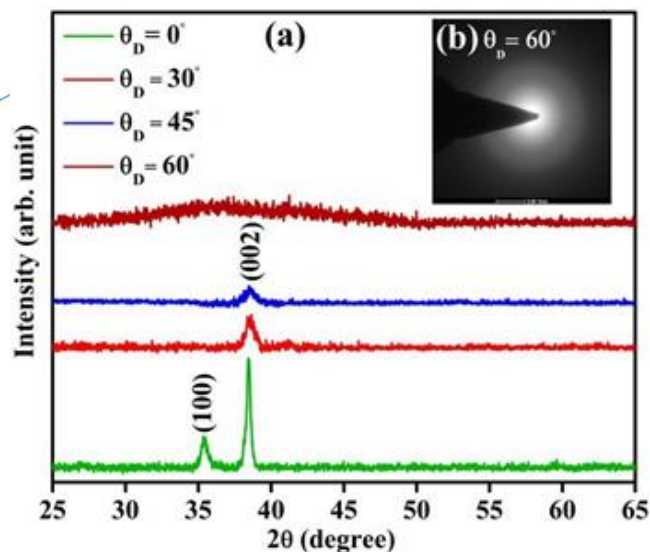


Fig. 2. (a) GA-XRD spectra of Ti thin films deposited at different deposition angles, $\theta_D = 0^\circ, 30^\circ, 45^\circ$ and 60° (Ref. JCPDS-ICDD no. 00-001-1197) and (b) SAED image for the sample $\theta_D = 60^\circ$ deposited on Si substrate.

Results and discussion

Structural analysis

Fig. 2(a) shows the XRD pattern of Ti thin films at various deposition angles $\theta_D = 0^\circ, 30^\circ, 45^\circ$ and 60° . The XRD analysis reveals that Ti thin films exhibited single crystalline for sample deposited at $\theta_D = 30^\circ$ and 45° as well as polycrystalline for sample deposited at $\theta_D = 0^\circ$ of hexagonal closed packed (HCP) structure with peaks at $2\theta = 35.03^\circ$ and 38.41° corresponding to (100) and (002) orientations, respectively (Ref. JCPDS-ICDD no. 00-001-1197). The dominant peak was obtained at 38.41° and is attributed to (002) plane. The reason for this highly intense (002) orientation is the low energy configuration

corresponding to this plane [26]. Further, with increase in the deposition angle from 0° to 45° , (002) orientation is suppressed and (100) is eliminated. However, the Ti thin film deposited at glancing angle of 60° shows amorphous nature. This may be attributed to the fact that the orientation of crystal planes is highly dependent on the growth rate along that plane.

Thus, chances of survival of the orientation with highest vertical growth rate will be high and the same will evolve as preferred orientation (002). Moreover, intensity of XRD peaks decreased with higher deposition angles, indicating that the degree of crystallinity in the Ti film is gradually decreased for larger inclination angle. This can be explained by the fact that the diffusion of deposited atoms is disturbed due to the shadowing effect during the glancing angle deposition [37]. Further, to confirm the amorphous nature, we have carried out TEM. Fig. 2(b) shows the SAED pattern of the sample deposited at $\theta_D = 60^\circ$, which confirmed the amorphous nature [41]. The amorphous nature may be due to the lower adatoms mobility at higher deposition angle. The average crystallite size of the samples (t) estimated using Scherer's formula [42] were found to be $\sim 27, 19$ and 11 nm for $\theta_D = 0^\circ, 30^\circ$ and 45° , respectively. Probable reasons for decrease in average particle size are shadowing effect at higher deposition angle [37].

Surface morphological analysis

The SEM micrographs of representative samples are shown in Fig. 3. These micrographs clearly reveal a change in the grain growth, size, and film packing density with respect to deposition angle. The average grain size and film thickness (~ 260 - 100 nm) were found to be decreased with higher deposition angle. The reduction in grain size and thickness may be due to the combined effect of decrease in area of cross-section for sputter atom flux and self-shielding effect during glancing angle deposition [35,37].

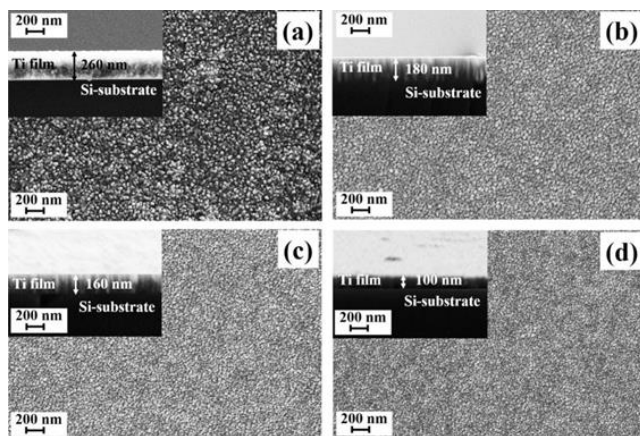


Fig. 3. FE-SEM images of Ti thin films with inset figure (which shows the cross sectional view of corresponding samples) at various deposition angles (a) 0° (b) 30° (c) 45° and (d) 60° .

Atomic force microscope (AFM) was also performed to study the morphological behavior and root mean square (rms) surface roughness of Ti films. Fig. 4 represents 2-D and 3-D AFM micrograph ($1 \mu\text{m} \times 1 \mu\text{m}$) of nanostructured Ti film as a function of deposition angle. AFM study revealed the spherical grain for samples deposited at $\theta_D =$

0° and columnar grain for samples deposited at $\theta_D = 30^\circ$ and 45° . However, for sample deposited at $\theta_D = 60^\circ$, columnar grain reposed on the surface by eliminating the porous structure. The rms surface roughness (δ_{rms}) were found to be $\sim 3, 28, 17$ and 2 nm for $\theta_D = 0^\circ, 30^\circ, 45^\circ$ and 60° , respectively. The increase in surface roughness is attributed to combine effect of small grain size and porous structure [43]. The overlapping of grain boundaries as well as disappearance of porosity leads to decrement in surface roughness.

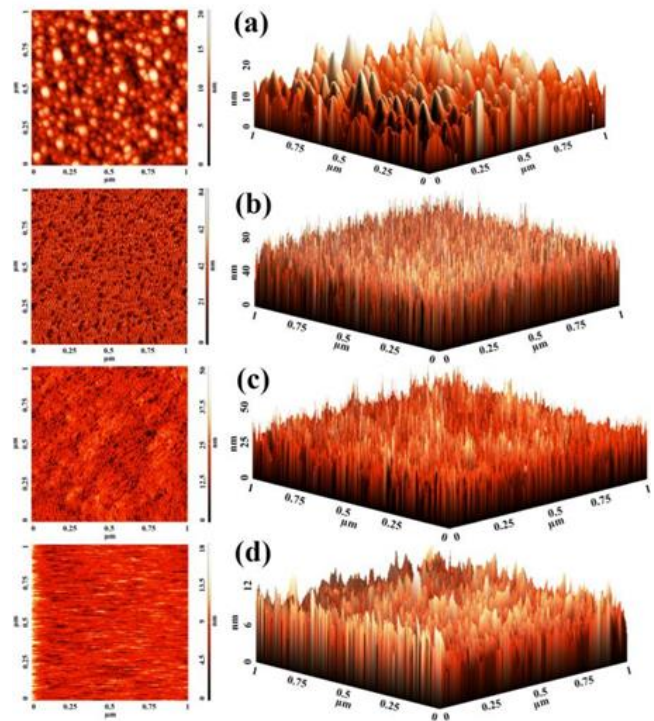


Fig. 4. 2-D and 3-D AFM images of Ti thin films deposited at various deposition angles (a) 0° (b) 30° (c) 45° and (d) 60° .

Wettability properties

In real world application, humidity (water molecules) stick down on the pure metal surface and change their physical, chemical and mechanical properties. The wettability on the surfaces was studied by Young [44]. He proposed a minimization model of three solid-vapour (γ_{sv}), solid-liquid (γ_{sl}) and liquid-vapour (γ_{lv}) phase interfacial energies (equation (1)).

$$\cos \theta_Y = \frac{\gamma_{sv} - \gamma_{sl}}{\gamma_{lv}} \quad (1)$$

where, θ_Y is characteristic water angle which depends on the interfacial energy at the contact area between the three phases (solid-liquid-air) and r_W is the roughness factor. The relation between surface morphology and the wettability explained by Young-Wenzel relation [45] given by equation (2).

$$\cos \theta_W = r_W \cos \theta_Y \quad (2)$$

where θ_w and r_{rms} is the water contact angle and the roughness factor respectively. If $\theta_w > 90^\circ$, surface is hydrophobic otherwise hydrophilic (**Fig. 5**).

The surface interfacial energy have polar and dispersive components and is related to contact angle by Young's equation [44]. Owens-Wendt and Wu presented the equations (3) and (4), respectively to calculate these two components of surface energy [46].

$$\gamma_{sl} = \gamma_{sv} + \gamma_{lv} - 2 \left(\sqrt{\gamma_{sv}^D \gamma_{lv}^D} + \sqrt{\gamma_{sv}^P \gamma_{lv}^P} \right) \quad (3)$$

$$\gamma_{sl} = \gamma_{sv} + \gamma_{lv} - 4 \left(\frac{\gamma_{lv}^D \times \gamma_{sv}^D}{\gamma_{lv}^D + \gamma_{sv}^D} + \frac{\gamma_{lv}^P \times \gamma_{sv}^P}{\gamma_{lv}^P + \gamma_{sv}^P} \right) \quad (4)$$

where γ_{lv}^D , γ_{sv}^D and γ_{lv}^P , γ_{sv}^P are the dispersive and polar components of liquid–vapour (γ_{lv}) energy and solid–vapour (γ_{sv}) energy, respectively. The surface energy of samples was determined by using two different fluids, water and diodomethane. **Table 1** lists the water contact angle and surface energy of samples calculated by above mentioned methods. The surface energies calculated by both methods were following same trend.

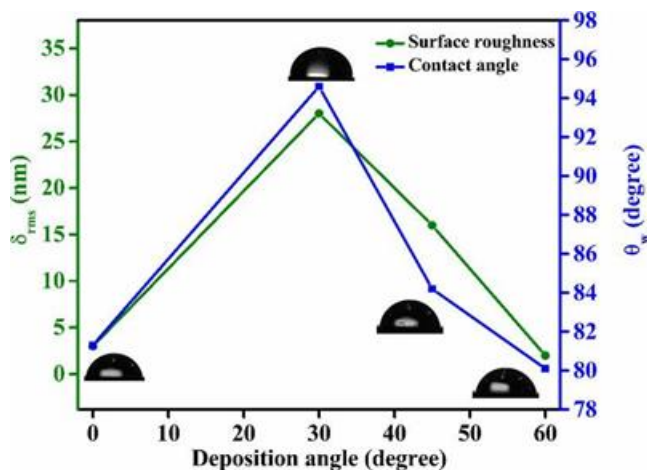


Fig. 5. Variation of rms surface roughness and water contact angle of deposited Ti films as a function of deposition angle.

Table 1. Calculated surface energy of representative samples.

Deposition angle (θ_D)	Contact angle (θ_w)	Method					
		Wu method			Owens method		
		γ_{sv} (mN/m)	γ_{sv}^D (mN/m)	γ_{sv}^P (mN/m)	γ_{sv} (mN/m)	γ_{sv}^D (mN/m)	γ_{sv}^P (mN/m)
0°	81.3°	31.35 (±2.04)	16.25 (±0.95)	15.10 (±1.31)	22.44 (±0.67)	10.89 (±0.29)	13.53 (±0.28)
30°	94.6°	22.89 (±1.87)	11.71 (±0.75)	11.18 (±1.12)	15.74 (±2.06)	7.01 (±2.06)	8.73 (±2.06)
45°	84.2°	29.55 (±2.01)	15.30 (±0.83)	14.26 (±1.18)	22.56 (±0.55)	10.05 (±0.28)	12.51 (±0.27)
60°	80.1°	32.43 (±2.06)	16.74 (±0.86)	15.52 (±1.22)	25.28 (±0.58)	11.32 (±0.30)	14.06 (±0.29)

Ti thin films were found to be hydrophilic in nature for the samples deposited at $\theta_D = 0^\circ$, 45° and 60° because of small surface roughness (~ 3 , 17 and 2 nm), respectively. The variation of surface roughness and water contact angle with deposition angle are shown in **Fig. 5**. The surface roughness determined from AFM results and water contact angle measurement has good agreement with Young-Wenzel relation (**Fig. 5**). The minimum surface energies

were observed for the sample exhibiting maximum surface roughness (~ 28 nm) and highest contact angle (~ 94.6) [46].

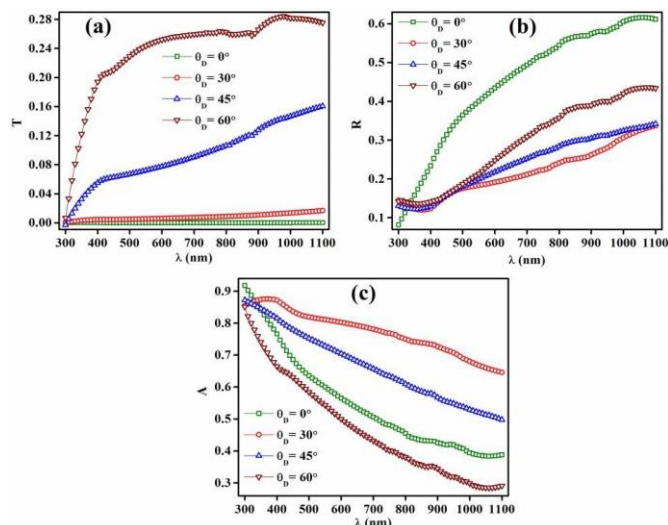


Fig. 6. Variation of (a) transmittance (b) reflectance and (c) absorbance with laser wavelength for Ti films deposited at various deposition angles.

Optical properties

Fig. 6(a) shows the variation of transmittance with wavelength in the range of 300 nm–1100 nm for Ti thin films fabricated at various deposition angles on glass substrates. From the transmittance curves, it is resolved that with increment in deposition angles, transmittance (0–28%) raises continuously over the wavelength range of 300–1100 nm. The results are attributed to combined effect of reduction in film thickness and particle size. **Fig. 6(b)** shows the plot of reflectance (R) spectra of the Ti thin films fabricated at different deposition angle. Reflectance of Ti thin films first decreases for the sample deposited at $\theta_D = 30^\circ$ and then increases upto $\theta_D = 60^\circ$. The high electron scattering at Fermi surface causes reduction in the reflection intensity, which leads to minimum reflectance (~ 12 –28%) for the sample ($\theta_D = 30^\circ$) exhibiting large surface roughness. Yin *et al* also reported that high surface roughness in thin films can lead to scattering (partially coherent propagation) within the films and results in substantial intensity reduction of reflectance [47]. Moreover, these results can also be explained by theoretical model (relation between surface roughness and optical properties if $\delta_{rms} \ll \lambda$), as given by equations (5) and (6), respectively [48].

$$R = \Delta R \left(\frac{\lambda}{4\pi \delta_{rms}} \right)^2 \quad (5)$$

$$T = \Delta T \left(\frac{\lambda}{2\pi \delta_{rms}} \right) (n_s - 1)^2 \quad (6)$$

where, ΔR , ΔT and n_s are the specular reflectance, transmittance and refractive index of substrate, respectively. **Fig. 6(c)** shows the variation of absorbance with wavelength of the Ti thin films. A large enhancement in NIR absorbance (~ 66 –75%) was found for the Ti thin

film deposited at $\theta_D = 30^\circ$. This result may be associated with multiple reflection and multiple absorption of the laser light due to large surface roughness, which enhance the absorption by an order of magnitude over a perfectly flat surface [29,48–50].

From the reflection spectra $R(\omega)$, we have calculated the loss angle $\phi(\omega)$, real (n) and imaginary (k) parts of refractive index of Ti thin films by using Kramers-Kronig relations (equations (7)-(9)) [29,51].

$$\phi(\omega) = -\frac{\omega}{\pi} P \int_0^\infty \frac{\ln R(\omega') - \ln R(\omega)}{\omega'^2 - \omega^2} d\omega' \quad (7)$$

$$n(\omega) = \frac{1 - R(\omega)}{1 + R(\omega) - 2\sqrt{R(\omega)} \cos \phi(\omega)} \quad (8)$$

$$k(\omega) = \frac{-2\sqrt{R(\omega)} \sin \phi(\omega)}{1 + R(\omega) - 2\sqrt{R(\omega)} \cos \phi(\omega)} \quad (9)$$

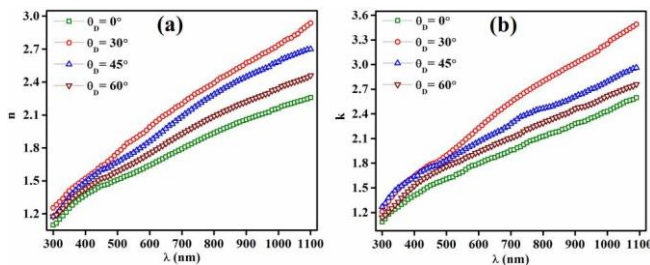


Fig. 7. The plot of (a) refractive index and (b) extinction coefficient with laser wavelength for representative samples, obtained from reflectance data using Kramers-Kronig relation.

Fig. 7(a) and **Fig. 7(b)** show the variation of refractive index and extinction coefficient with wavelength at various deposition angles, respectively. An increasing trend was observed for both refractive index and extinction coefficient with respect to the wavelength. The sample with maximum surface roughness and hydrophobic nature, exhibits highest value of refractive index and extinction coefficient. These results may be associated with scattering of the laser light within the films due to large surface roughness [47]. **Table 2** lists the values of refractive index and extinction coefficient at different wavelengths.

Table 2. The refractive index (n) and extinction coefficient (k) of Ti thin films.

Deposition angle (θ_D)	Optical constant (n and k) of Ti thin films for different laser wavelength							
	$\lambda = 630 \text{ nm}$		$\lambda = 940 \text{ nm}$		$\lambda = 980 \text{ nm}$		$\lambda = 1060 \text{ nm}$	
	n	k	n	k	n	k	n	k
0°	1.686	1.847	2.098	2.330	2.144	2.401	2.221	2.555
30°	2.063	2.329	2.634	3.101	2.700	3.208	2.839	3.414
45°	1.928	2.124	2.501	2.680	2.562	2.751	2.662	2.910
60°	1.803	1.993	2.267	2.506	2.321	2.576	2.411	2.714

In addition to the dependence of above studied properties on the deposition angle, it is worth here to mention that, the variation in glancing angle during deposition may vary the kinetic energy of Ti ions, ion flux and plasma induced substrate temperature and will have a direct consequence on the observed properties. It is well-known that, the sputtering of atoms is caused by positive ions which are accelerated toward the target within the plasma sheath. The interactions between these positive ions and the target material are very complex. The kinetic energy distribution and the directionality of the sputtered atoms can be drastically altered by the collisions taking

place between the sputtered target atoms and the species of the plasma, even if they leave the target with energies in the order of 1-10 eV and high preferential directionality. Therefore, it is difficult to draw an analytical relation between the parameters like kinetic energy, ion flux and plasma induced substrate temperature, and the deposition parameters due to the complexity of the mechanism involved in this process. However, to simplify the description and to deduct general analytic relations, Alvarez *et al.* have successfully applied the effective thermalizing collision (ETC) approximation to describe the collisional transport of sputtered particles in plasma [52].

A comparison of the present work with previous studies on Ti thin films have been shown in **Table 3**. It can be realized that the present work has explored the possible effects of deposition angle on the absorption properties of Ti thin films in the UV-Vis-NIR region as well as the wettability of films which were remain untouched in the previous studies. Thus, in the present work, a correlation between the deposition angle and surface roughness of the Ti thin films reveals that the wettability and absorption, which are highly dependent on the surface roughness, can be easily tuned by the deposition angle.

Table 3. A comparison of the present work with previous studies on Ti thin films.

	Ref. [29]	Ref. [28]	Ref. [26]	Ref. [22,28]	Ref. [30]	Ref. [31]	Ref. [40]	Ref. [39]	Present W
Technique	magnetron sputtering	magnetron sputtering	magnetron sputtering	magnetron sputtering	electron beam evaporation	electron beam evaporation	electron beam evaporation	electron beam evaporation	magnetron sputtering
Glancing angle	×	×	×	×	√	√	×	√	√
Properties/Applications	morphology and optical	optical/hydrogen storage and sensor	electrical, structural, optical and surface	Optical and wettable	surface roughness	surface roughness	optical	optical	structure morphology optical at wettable
Wavelength range explored				UV-Vis (300-800 nm) range only				UV-Vis-NIR range (300-1100 nm)	

Conclusion

The nanostructured Ti thin films were deposited by varying deposition angle on glass and Si substrates by magnetron sputtering. It was found that microstructure and morphology of Ti thin films are highly dependent on deposition angle. The average grain size ($\sim 27 \text{ nm}$ - 11 nm) and film thickness ($\sim 260 \text{ nm}$ - 100 nm) were found to decrease with increase in deposition angle. Columnar growth and porous structure was obtained for the sample fabricated at deposition angle $\theta_D = 30^\circ$. Using AFM analysis, it was observed that the surface roughness changes with deposition angle. Maximum roughness was found for the sample with $\theta_D = 30^\circ$. The tuning of transmittance, reflectance and absorbance of Ti thin films with deposition angle has been investigated. Large absorbance (~ 66 - 75%) and minimum reflectance (~ 22 - 30%) with the highest n and k values have been achieved in NIR range for the sample exhibiting maximum surface roughness deposited at $\theta_D = 30^\circ$. A hydrophobic nature of Ti thin film was observed for the sample fabricated at $\theta_D = 30^\circ$. It was observed that the surface roughness followed the same trend as absorbance and water contact angle. Good optical absorbance along with hydrophobic character make Ti thin films of great use as photon absorbing layer for photonic and biomedical devices.

Acknowledgements

This work has been supported by the grant no. ARMREB/CDSW/2013/152, Government of India, Ministry of Defence.

One of the authors, Jyoti Jaiswal, would like to thank Ministry of Human Resource and Development, India for providing the financial assistance.

Reference

- Parida, Kaur, G.; Mitra, A.; Yadav, K. L.; *Adv. Mater. Lett.*, **2015**, *6*, 73.
DOI: [10.5185/amlett.2015.5606](https://doi.org/10.5185/amlett.2015.5606)
- Kariper, İ. A.; *Opt. Mater.*, **2015**, *40*, 78.
DOI: [10.1016/j.optmat.2015.03.012](https://doi.org/10.1016/j.optmat.2015.03.012)
- Singh, P.; Srivatsa, K. M. K.; Das, S.; *Adv. Mater. Lett.*, **2015**, *6*, 371.
DOI: [10.5185/amlett.2015.5777](https://doi.org/10.5185/amlett.2015.5777)
- Signore, M. A.; Sytchkova, A.; Dimairo, D.; Cappello, A.; Rizzo, A.; *Opt. Mater.*, **2012**, *34*, 632.
DOI: [10.1016/j.optmat.2011.09.012](https://doi.org/10.1016/j.optmat.2011.09.012)
- Khalifa, N.; Kaouach, H.; Chtourou, R.; *Opt. Mater.*, **2015**, *45*, 9.
DOI: [10.1016/j.optmat.2015.03.003](https://doi.org/10.1016/j.optmat.2015.03.003)
- Hoang, T. T. Q.; The, N. D.; McVitie, S.; Nam, N. H.; Vu, L. V.; Canh, T. D.; Long, N. N.; *Opt. Mater.*, **2011**, *33*, 308.
DOI: [10.1016/j.optmat.2010.09.008](https://doi.org/10.1016/j.optmat.2010.09.008)
- Duan, N.; Lin, H.; Li, L.; Hu, J.; Bi, L.; Lu, H.; Weng, X.; Xie, J.; Deng, L.; *Opt. Mater. Express*, **2013**, *3*, 1537.
DOI: [10.1364/OME.3.001537](https://doi.org/10.1364/OME.3.001537)
- Misheva, M.; Djourelov, N.; Kotlarova, T.; Elenkov, D.; Passage, G.; *Thin Solid Films*, **1996**, *283*, 26.
DOI: [10.1016/0040-6090\(95\)08493-2](https://doi.org/10.1016/0040-6090(95)08493-2)
- Sultana, T.; Newaz, G.; Georgiev, G. L.; Baird, R. J.; Auner, G. W.; Patwa, R.; Herfurth, H. J.; *Thin Solid Films*, **2010**, *518*, 2632.
DOI: [10.1016/j.tsf.2009.08.004](https://doi.org/10.1016/j.tsf.2009.08.004)
- Tsuchiya, T.; Hirata, M.; Chiba, N.; *Thin Solid Films*, **2005**, *484*, 245.
DOI: [10.1016/j.tsf.2005.02.024](https://doi.org/10.1016/j.tsf.2005.02.024)
- Xue, X.; Wang, S.; Zeng, C.; Bai, H.; Li, L.; Wang, Z.; *Surf. Coat. Technol.*, **2014**, *244*, 151.
DOI: [10.1016/j.surfcoat.2014.01.064](https://doi.org/10.1016/j.surfcoat.2014.01.064)
- Song, Y. H.; Cho, S. J.; Jung, C. K.; Bae, I. S.; Boo, J. H.; *J. Korean Phys. Soc.*, **2007**, *51*, 1152.
DOI: [10.3938/jkps.51.1152](https://doi.org/10.3938/jkps.51.1152)
- Atuchin, V. V.; Ziling, C. C.; Shipilova, D. P.; Beizel, N. F.; *Ferroelectrics*, **1989**, *100*, 261.
DOI: [10.1080/00150198908007921](https://doi.org/10.1080/00150198908007921)
- Fujitsuka, N.; Sakata, J.; Miyachi, Y.; Mizuno, K.; Ohtsuka, K.; Taga, Y.; Tabata, O.; *Sens. Actuators, A*, **1998**, *66*, 237.
DOI: [10.1016/S0924-4247\(98\)00050-8](https://doi.org/10.1016/S0924-4247(98)00050-8)
- Hofmann, K.; Spangenberg, B.; Luysberg, M.; Kurz, H.; *Thin Solid Films*, **2003**, *436*, 168.
DOI: [10.1016/S0040-6090\(03\)00582-0](https://doi.org/10.1016/S0040-6090(03)00582-0)
- Lüdecke, C.; Bossert, J.; Roth, M.; Jandt, K. D.; *Appl. Surf. Sci.*, **2013**, *280*, 578.
DOI: [10.1016/j.apsusc.2013.05.030](https://doi.org/10.1016/j.apsusc.2013.05.030)
- Ogawa, S.; Kouzaki, T.; Yoshida, T.; Sinclair, R.; *J. Appl. Phys.*, **1991**, *70*, 827.
DOI: [10.1063/1.349641](https://doi.org/10.1063/1.349641)
- Ramakrishna, M. V. S.; Karunasiri, G.; Neuzil, P.; Sridhar, U.; Zeng, W. J.; *Sens. Actuators, A*, **2000**, *79*, 122.
DOI: [10.1016/S0924-4247\(99\)00280-0](https://doi.org/10.1016/S0924-4247(99)00280-0)
- David, T. O.; S.E. Rodil; S. Muhl.; *Mater. Sci.*, **2008**, *14*, 15.
- Whitehead, K. A.; Verran, J.; *Int. Biodeterior. Biodegrad.*, **2007**, *60*, 74.
DOI: [10.1016/j.ibiod.2006.11.009](https://doi.org/10.1016/j.ibiod.2006.11.009)
- Kruger, V. G.; Kalenskii, A. V.; Zvekov, A. A.; Zykov, I. Y.; Aduv, B. P.; *Combust. Explos. Shock Waves*, **2012**, *48*, 705.
DOI: [10.1134/S001050821206007X](https://doi.org/10.1134/S001050821206007X)
- Soethe, V. L.; Nohara, E. L.; Fontana, L. C.; Rezende, M. C.; *J. Aerosp. Technol. Manag.*, **2011**, *3*, 279.
DOI: [10.5028/jatm.2011.03030511](https://doi.org/10.5028/jatm.2011.03030511)
- Kennedy, J. E.; Early, J. W.; Thomas, K. A.; Lester, C. S.; 28th International Pyrotechnics Seminar, Adelaide, Australia, Nov. 4-9, **2001**.
- Fang, V.; Kennedy, J. V.; Futter, R. J.; Manning, J.; *GNS Science Report*, **2013**, *39*, 23.
- Apreutesei, M.; Lopes, C.; Borges, J.; Vaz, F.; Macedo, F.; *J. Vac. Sci. Technol. A*, **2014**, *32*, 041511.
DOI: [10.1116/1.4884351](https://doi.org/10.1116/1.4884351)
- Jeyachandran, Y. L.; Karunakaran, B.; Narayandass, S. K.; Mangalaraj, D.; *Mater. Sci. Eng. A*, **2007**, *458*, 361.
DOI: [10.1016/j.msea.2006.12.088](https://doi.org/10.1016/j.msea.2006.12.088)
- Scardi, P.; Leoni, M.; Checchetto, R.; *Mater. Lett.*, **1998**, *36*, 1.
DOI: [10.1016/S0167-577X\(97\)00286-3](https://doi.org/10.1016/S0167-577X(97)00286-3)
- Singh, M.; Srivastava, S.; Agarwal, S.; Kumar, S.; Vijay, Y. K.; *Bull. Mater. Sci.*, **2010**, *33*, 569.
DOI: [10.1007/s12034-010-0087-8](https://doi.org/10.1007/s12034-010-0087-8)
- Einollahzadeh-Samadi, M.; Dariani, R. S.; *Appl. Surf. Sci.*, **2013**, *280*, 263.
DOI: [10.1016/j.apsusc.2013.04.146](https://doi.org/10.1016/j.apsusc.2013.04.146)
- Backholm, M.; Foss, M.; Nordlund, K.; *Nanotechnology*, **2012**, *23*, 385708.
DOI: [10.1088/0957-4484/23/38/385708](https://doi.org/10.1088/0957-4484/23/38/385708)
- Backholm, M.; Foss, M.; Nordlund, K.; *Appl. Surf. Sci.*, **2013**, *268*, 270.
DOI: [10.1016/j.apsusc.2012.12.077](https://doi.org/10.1016/j.apsusc.2012.12.077)
- Barranco, A.; Borrás, A.; Gonzalez-Elipe, A. R.; Palmero, A.; *Prog. Mater. Sci.*, **2016**, *76*, 59.
DOI: [10.1016/j.pmatsci.2015.06.003](https://doi.org/10.1016/j.pmatsci.2015.06.003)
- Jie, N.; Yu, Z.; Qin, Z.; Zhengjun, Z.; *J. Am. Ceram. Soc.*, **2008**, *91*, 3458.
DOI: [10.1111/j.1551-2916.2008.02654.x](https://doi.org/10.1111/j.1551-2916.2008.02654.x)
- Khedir, K. R.; *Phys. Lett. A*, **2010**, *374*, 4430.
DOI: [10.1016/j.physleta.2010.08.066](https://doi.org/10.1016/j.physleta.2010.08.066)
- Poxson, D. J.; Mont, F. W.; Schubert, M. F.; Kim, J. K.; Schubert, E. F.; *Appl. Phys. Lett.*, **2008**, *93*, 101914.
DOI: [10.1063/1.2981690](https://doi.org/10.1063/1.2981690)
- Wisitsoorat, A.; *Sensors Actuators B Chem.*, **2013**, *182*, 795.
DOI: [10.1016/j.snb.2013.03.091](https://doi.org/10.1016/j.snb.2013.03.091)
- Leem, J. W.; Yu, J. S.; *Opt. Express*, **2011**, *19*, 258.
DOI: [10.1364/OE.19.00A258](https://doi.org/10.1364/OE.19.00A258)
- Ivanova, E. P.; Truong, V. K.; Wang, J. Y.; Berndt, C. C.; Jones, R. T.; Yusuf, I. I.; Peake, I.; Schmidt, H. W.; Fluke, C.; Barnes, D.; Crawford, R. J.; *Langmuir*, **2010**, *26*, 1973.
DOI: [10.1021/la902623c](https://doi.org/10.1021/la902623c)
- Kangarlow, H.; Aghgonbad, M. M.; Calculation of Optical Parameters of Titanium Nano-layers with Different Deposition Angles, Proc. WCE, London, U.K., Vol. II, **2011**.
- Kangarlow, H.; Aghgonbad, M. M.; *Ukr. J. Phys. Opt.*, **2012**, *13*, 4.
- Balakrishnan, G.; Tripura Sundari, S.; Ramaseshan, R.; Thirumurugesan, R.; Mohandas, E.; Sastikumar, D.; Kuppusami, P.; Kim, T. G.; Song, J. I.; *Ceram. Int.*, **2013**, *39*, 9017.
DOI: [10.1016/j.ceramint.2013.04.104](https://doi.org/10.1016/j.ceramint.2013.04.104)
- Cullity, B. D. (Eds. 1st); Elements of X Ray Diffraction, Reading, MA: Addison-Wesley, **1956**, 99.
DOI: [10.1017/CBO9781107415324.004](https://doi.org/10.1017/CBO9781107415324.004)
- Dave, V.; Dubey, P.; Gupta, H. O.; Chandra, R.; *Thin Solid Films*, **2013**, *549*, 2.
DOI: [10.1016/j.tsf.2013.07.016](https://doi.org/10.1016/j.tsf.2013.07.016)
- Young, T.; *Philos. Trans. R. Soc. London*, **1805**, *95*, 65.
DOI: [10.1098/rstl.1805.0005](https://doi.org/10.1098/rstl.1805.0005)
- Wenzel, R. N.; *Ind. Eng. Chem.*, **1936**, *28*, 988.
DOI: [10.1021/ie50320a024](https://doi.org/10.1021/ie50320a024)
- Sanger, A.; Kumar, A.; Chauhan, S.; Gautam, Y. K.; Chandra, R.; *Sens. Actuators, B*, **2015**, *213*, 252.
DOI: [10.1016/j.snb.2015.02.098](https://doi.org/10.1016/j.snb.2015.02.098)
- Yin, G.; Merschjann, C.; Schmid, M.; *J. Appl. Phys.*, **2013**, *113*, 213510-1.
DOI: [10.1063/1.4809550](https://doi.org/10.1063/1.4809550)
- Bennett, H. E.; Burge, D. K.; *J. Opt. Soc. Am.*, **1980**, *70*, 268.
DOI: [10.1364/JOSA.70.000268](https://doi.org/10.1364/JOSA.70.000268)
- Yamada, Y.; Bao, S.; Tajima, K.; Okada, M.; Yoshimura, K.; Roos, A.; *Sol. Energy Mater. Sol. Cells*, **2008**, *92*, 1617.
DOI: [10.1016/j.solmat.2008.07.011](https://doi.org/10.1016/j.solmat.2008.07.011)
- Fedders, P. A.; *Phys. Rev.*, **1969**, *181*, 1053.
DOI: [10.1103/PhysRev.181.1053](https://doi.org/10.1103/PhysRev.181.1053)
- Lichvar, P.; Liska, M.; Galusek, D.; *Ceram.-Silik.*, **2002**, *46*, 25.
- Alvarez, R.; Garcia-Martin J. M.; Macias-Montero, M.; Gonzalez-Garcia, L.; Gonzalez, J. C.; Rico V.; Perlich, J.; Cotrino, J.; Gonzalez-Elipe, A. R.; Palmero, A.; *Plasma Process. Polym.*, **2014**, *11*, 571.

